High Gain, Load-Tolerant Self-Powered Series–Parallel Synchronized Switching Technique for Piezoelectric Energy Harvesting

Mickaël Lallart

***Abstract*—In the framework of autonomous wireless devices (*e.g.*, sensors) powered by energy available from their surrounding environment, this article exposes a technique combining the so-called series and parallel Synchronized Switch Harvesting on Inductor (SSHI) approaches for piezoelectric energy harvesting. More specifically, the proposed circuit consists in switching the piezoelectric element on two inductors, one in series between the piezoelement and the energy extraction stage (rectifier bridge) and the other one in parallel with the rectifier. This, therefore, allows several energy transfer processes to occur per half period, even when the switching process is finished. Based on numerical analysis supported by experimental validations, it is shown that such a technique permits a significant widening of the effective load and rectified voltage ranges, but also, under particular conditions, a power output magnification that is even larger than in the sole SSHI case.**

***Index Terms*—Energy conversion, energy harvesting, piezoelectric devices, switched circuits.**

I. Introduction

With the exponential spreading of connected devices such as wireless sensors and sensor networks, a significant pressure on their power supply has raised. While primary batteries remain the conventional way for providing energy to these systems, their implementation and use is facing tighter and tighter constraints. More precisely, the strongest limitation of such a solution has experienced a change of paradigm with the development of ultralow-power circuits that consume very little energy. Hence, while initial concerns considered the actual energy initially stored in batteries, the main limiting factors now lie in the battery leakage, yielding a loss of energy before it is actually used [1], [2]. Such an issue is even more dramatic in relatively harsh environments. For instance, under an ambient temperature of 60° C, Li-Ion batteries show a drop of their energy by more than 60% over one year [1]. Hence, such a solution is not realistically applicable for devices aiming at operating on the long run in confined environments or under moderately severe conditions.

As an alternative to these battery-powered solutions, collecting energy from the direct surroundings of the device, namely energy harvesting, has been the topic of many works since two decades [3], [4] in its modern form. Ambient sources may consider solar, thermal, or vibrational energy for instance. Due to its ubiquity and constant availability, the latter is an attractive choice for microgenerators. The conversion of the mechanical energy into electricity can be achieved through electromagnetic, piezoelectric, or electrostatic coupling for instance [5]. In the framework of small energy harvesters with centimeter-scale dimensions, piezoelectric coupling is of particular interest thanks to good integration potentials and relatively high power densities.

Nevertheless, when integrating the active material on the structure, and especially considering cost-effective transducers, the global electromechanical coupling at the structural level is usually limited to a few percent. Therefore, means of improving the conversion efficiency is mandatory in order to achieve sufficient output power levels. From the electrical perspective, such an achievement can be obtained thanks to a nonlinear process that consists in switching the piezoelectric transducer on an inductance each time an extremal voltage or displacement is detected. This technique, called "Synchronized Switch Harvesting on Inductor" (SSHI), allows thanks to an voltage inversion effect (permitted by the resonant circuit made of the inductor and piezoelectric capacitance during the switching event) a magnification of the piezovoltage as well as a reduced phase shift between the voltage and velocity [7], [8]. These two combined effects, thus, contribute to an artificial increase of the electromechanical coupling, allowing a significant gain in terms of harvested power by a factor up to ten compared to the standard approach (sole rectifier bridge). SSHI can be implemented with the switching element either in parallel [7] or in series [8], [9]. For integration purposes, the inductor can be advantageously replaced by another high frequency piezoelectric oscillator, providing kinetic energy storage by mechanical means [10]. Furthermore, the SSHI can be made totally self-powered, thus working in a realistic fashion using a very small amount of the electrostatic energy available on the piezoelement [11]–[16]. Nevertheless, in order to benefit from this power output boosting effect, the load should be carefully tuned in a similar way than in standard approach, requiring the use of additional load

Manuscript received August 1, 2021; revised November 11, 2021; accepted January 31, 2022. Date of publication February 11, 2022; date of current version March 24, 2022. This work was supported by the Institut Carnot Ingénierie@Lyon under the IMPACT Project. Recommended for publication by Associate Editor B. Semail.

Mickaël Lallart is with INSA-Lyon, University of Lyon, F-69621 Villeurbanne, France, and also with LGEF INSA-Lyon, University of Lyon, 69621 Villeurbanne Cedex, France (e-mail: mickael.lallart@insa-lyon.fr).

Color versions of one or more figures in this article are available at https://doi.org/10.1109/TPEL.2022.3150410.

Digital Object Identifier 10.1109/TPEL.2022.3150410

adaptation stages, for instance based on dc/dc converters (*e.g.*, step-down–[17]–or buck–boost–[18], [19]), yielding further energy losses. More precisely, the series implementation of the switching element (w.r.t. the transducer and the rectifier) yields a decreased optimal load compared to the standard technique while the parallel approach increases it.

To address this load adaptation issue and still based on the switching concept, the "Synchronous Electric Charge Extraction" (SECE) technique has been proposed by Lefeuvre *et al.* [20], [21]. Contrary to the SSHI approach, the switch is reopened when the piezovoltage cancels in the SECE. This allows transferring all of the electrostatic energy available on the piezoelement to the inductance, which is latter transferred to the load and storage capacitor. Thanks to this process, the load is never directly connected to the piezoelement, hence allowing a harvested energy independent from the connected load. However, SECE shows a lower gain compared to SSHI (typically around three w.r.t. standard interface and taking into account losses in the energy transfer), and its self-powered implementation is much more complex [22]. While some techniques, such as Double Synchronized Switch Harvesting (DSSH–[23]), Enhanced Synchronized Switch Harvesting (ESSH–[24]), hybrid SSHI [25], optimized SECE [26], or Synchronous Inversion and Charge Extraction (SICE) [27], [28], have been proposed to combine the advantages of SSHI and SECE, they still suffer from some of the drawbacks of SSHI (load dependence) and/or SECE (limited gain, complex implementation), or can raise other issues, such as integrability (e.g., due to the need of electromagnetic transformer).

Hence, the purpose of this article is to expose a simple approach for combining, to some extent, a significant power gain (compared to maximal power of the standard approach) over a wide load range while keeping the simplicity of implementation of SSHI (self-powering abilities). The principles behind the proposed technique lie in separating the switching inductor of the SSHI into two inductors, with one placed between the piezoelectric element (PZT) and the rectifier and the second in parallel with the rectifier. This, therefore, can be seen as a combination of series and parallel SSHI (with however some aspects from the SECE as it will be devised in the followings), leading to the concept of "series–parallel SSHI" (sp-SSHI).

The rest of this article is organized as follows. Section II aims at exposing the basic operations of the proposed concept, which are theoretically investigated in Section III. Then, the performance of the circuit is numerically evaluated in Section IV and compared with other techniques. Before a short conclusion recalling the main parts of this article, the experimental operations are evaluated in Section V, including the self-powered version assessment. Finally, Section VI concludes this article.

II. Principles

The concept of the series–parallel SSHI (sp-SSHI) lies in splitting the switching inductance, and placing one part in series with the energy extraction stage (rectifier) made of diodes D_1 and D_2 as well as smoothing capacitors C_1 and C_2 and the other part in parallel to it, resulting in the schematic depicted in Fig. 1.

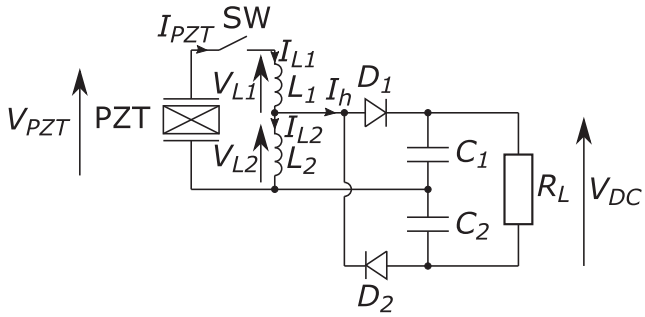

Fig. 1. sp-SSHI circuit.

$V_{\rm PZT}$, V_{L1}, and V_{L2} refer to the voltage across the piezoelectric element (PZT), inductor L_1 and inductor L_2, respectively, while $V_{\rm DC}$ denotes the rectified voltage across the resisitive load R_L. $I_{\rm PZT}$, I_{L1}, and I_{L2} are the current flowing out the PZT and currents through inductors L_1 and L_2, respectively. Finally, I_h represents the current flowing through the storage stage, hence corresponding to the harvested charge flow. Note that instead of a full-wave voltage doubler, a full diode bridge rectifier may be also used, but would increase losses due to the supplementary diodes (as well as decreasing the optimal resistor). With such a configuration, current can flow from the PZT through the rectifier (series SSHI operations–[8]), but at the same time, the parallel inductance L_2 may see its voltage clamped by half the value of the rectified one as for parallel SSHI configuration [7]. Additionally, there might be some residual current in the inductance L_2 after the inversion process, that can be further harvested as in the SECE approach [20].

More precisely, the different steps in the process are exposed in Figs. 2 and 3. Most of the time, the piezoelement is left in open circuit, with its voltage varying with the displacement (states ⓐ for positive voltages and ⓕ for negative ones). Once an extremal voltage occurs, the switch SW is turned ON so that current is flowing from the piezomaterial to the inductances. However, in the case the voltage across the inductor L_2 is higher, in absolute value, than half the rectified voltage $V_{\rm DC}/2$ (or in other words the absolute piezovoltage is greater than $(1 + L_1/L_2)V_{\rm DC}$), the voltage across inductance L_2 is clipped to $\pm V_{\rm DC}/2$ and so is the rate of the current flowing through this inductor. Consequently, part of the piezocurrent is flowing through the rectifier bridge (I_h), yielding a first step in the harvesting process (states ⓑ for switching event from positive voltage switch and ⓖ for switching event from negative voltage). When the two inductor currents, namely I_{L1} for L_1 and I_{L2} for L_2, equal each other, the rectifier stops conducting and the piezocurrent is solely flowing through L_1 and L_2 (also yielding a change in the inversion frequency–states ⓒ and ⓗ). However, as the current through L_2 decreases, it may eventually yield a sufficient reverse voltage so that the other part of the rectifier is conducting (states ⓓ and ⓘ), also contributing to the harvesting process. Finally, due to the current rate limitation of L_2, I_{L2} may not be zero when I_{L1} cancels (end of the piezovoltage inversion). Consequently, a supplementary harvesting event may go beyond the inversion process (states ⓔ and ⓙ) before going back to state ⓕ or ⓐ

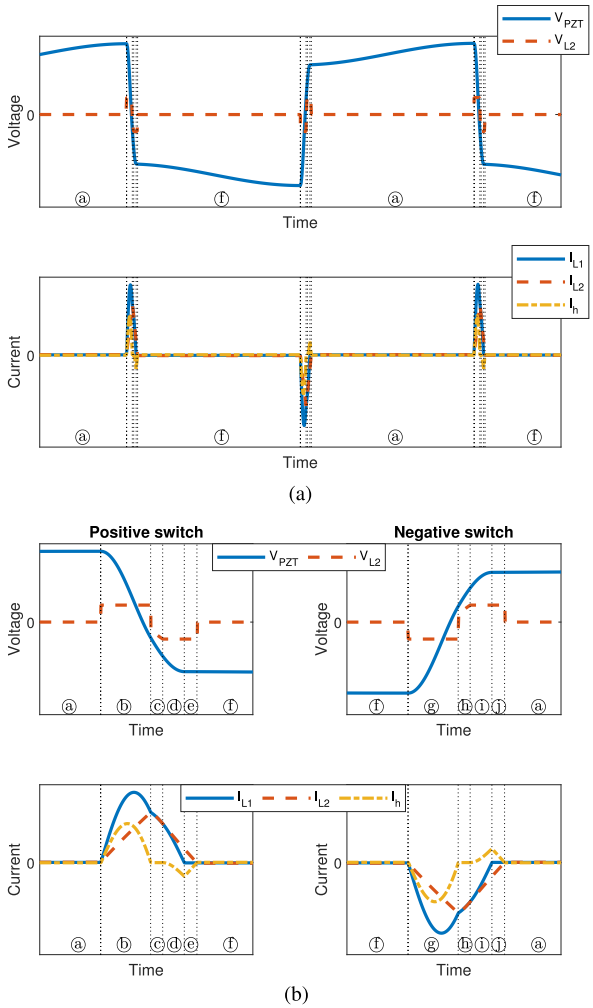

Fig. 2. sp-SSHI typical waveforms. (a) Global view. (b) Enlargements around switching events.

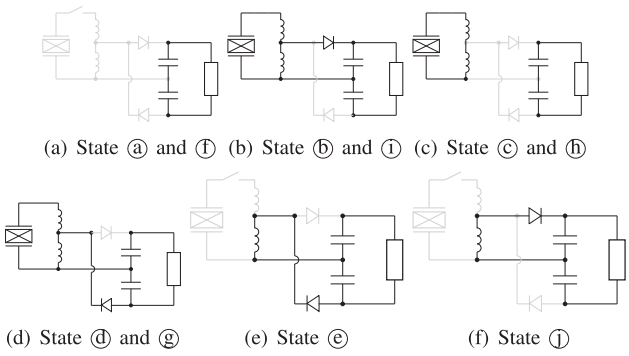

Fig. 3. Circuit states during operations.

Compared to other variants of SSHI and/or SECE and as it will be devised in the followings, the interest of the sp-SSHI lies in the following.

1) Significant power gain due to the voltage inversion, instead of cancellation in the case of SECE and associated techniques [20], [26].
2) Simple implementation thanks to a single switching stage that can be easily self-powered as the switching process ends on piezoelectric current cancellation, contrary to DSSH [23], ESSH [24], or SICE [27], for instance, which implement several switching sequences, with at least one requiring termination on maximum current that yields complex self-powered implementation.
3) Relative integrability, while hybrid SSHI (combining parallel SSHI and SSHI-MR–[25]) for example, requires a bulky transformer.
4) Significant power for a load range covering both series and parallel, while hybrid SSHI [25] is not adapted to relatively low loads values.

III. Analysis

In the following, the numerical analysis of the sp-SSHI is proposed. For the sake of simplicity and in order to concentrate on the circuit itself, it will be considered that the piezoelectric structure features constant displacement magnitude so that no damping effect will be considered. While this assumption is valid for weakly coupled and/or strongly damped devices, or when the excitation frequency is sufficiently far away from the resonance frequency, it is, however, possible to take into account the damping effect induced by the harvesting process by using Mason electromechanical model [29] for instance. Additionally, it will be considered that the smoothing capacitors C_1 and C_2 are large enough so that the time constant defined by these capacitors and the load R_L is much larger than the vibration period, yielding an almost constant value of the rectified voltage $V_{\rm DC}$.

Under the considered hypotheses, only the piezoelectric electrical equation can be considered. Using a lumped model representation [30], this turns to a velocity controlled current source with a capacitive internal impedance as

$$I_{\rm PZT}(t) = \alpha \dot{u}(t) - C_0 \dot{V}_{\rm PZT}(t) \tag{1}$$

where $I_{\rm PZT}(t)$ and $V_{\rm PZT}(t)$ are the outgoing piezocurrent and piezovoltage, respectively, $u(t)$ the structure flexural displacement, and α and C_0 the force factor and clamped capacitance, respectively.

A. State Equations

For setting up the numerical description of the sp-SSHI operations, the state vector $\mathbf{Y}(t)$ made of the piezoelectric voltage $V_{\rm PZT}(t)$, and the currents flowing through inductors L_1 and L_2, namely $I_{L1}(t)$ and $I_{L2}(t)$, respectively, will be considered

$$\mathbf{Y}(t) = \begin{pmatrix} V_{\rm PZT}(t) \\ I_{L1}(t) \\ I_{L2}(t) \end{pmatrix} \tag{2}$$

while the input vector $\mathbf{X}(t)$ is dependent on the structure displacement $u(t)$ and rectified voltage $V_{\rm DC}$ (recalling the latter is assumed constant)

$$\mathbf{X}(t) = \begin{pmatrix} u(t) \\ V_{\rm DC} \end{pmatrix}. \tag{3}$$

Based on this model, the derivative of state vector $\mathbf{Y}$, denoted $\dot{\mathbf{Y}}$ can be written as

$$\dot{\mathbf{Y}}(t) = \mathbf{A}_x \mathbf{Y}(t) + \mathbf{B}_x \mathbf{X}(t) \tag{4}$$

with $\mathbf{A}_x$ and $\mathbf{B}_x$ the respective 3×3 and 3×2 state matrices, where the subscript x denotes the state (ⓐ to ⓙ, as defined in Fig. 3).

In nonswitching state and without conduction (states ⓐ and ⓕ, no current is flowing in the whole circuit (except from the storage capacitor to the load, which is not to be taken into account here as the rectified voltage V_{DC} is assumed constant). Therefore, the expression of the associated state matrices leads to the following expressions:

$$\mathbf{A_a} = \mathbf{A_f} = \begin{bmatrix} 0 & 0 & 0 \\ 0 & 0 & 0 \\ 0 & 0 & 0 \end{bmatrix}$$
$$\mathbf{B_a} = \mathbf{B_f} = \begin{bmatrix} \frac{\alpha}{C_0} & 0 \\ 0 & 0 \\ 0 & 0 \end{bmatrix}. \tag{5}$$

Once an extremum value is reached, the switch SW is closed. Therefore, a current is flowing from the piezoelement to the inductors. However, the current rate through L_2 is limited due to the conduction of the rectifier bridge, that clips the voltage across L_2 to $V_{\text{DC}}/2$ for switching from positive voltage (state ⓑ) or $-V_{\text{DC}}/2$ when the switching starts from a negative voltage (state ⓖ). This yields the following definition of the state matrices:

$$\mathbf{A_b} = \mathbf{A_g} = \begin{bmatrix} 0 & -\frac{1}{C_0} & 0 \\ \frac{1}{L_1} & -\frac{r_1}{L_1} & 0 \\ 0 & 0 & -\frac{r_2}{L_2} \end{bmatrix}$$
$$\mathbf{B_b} = \begin{bmatrix} \frac{\alpha}{C_0} & 0 \\ 0 & -\frac{1}{2L_1} \\ 0 & \frac{1}{2L_2} \end{bmatrix}; \mathbf{B_g} = \begin{bmatrix} \frac{\alpha}{C_0} & 0 \\ 0 & \frac{1}{2L_1} \\ 0 & -\frac{1}{2L_2} \end{bmatrix}. \tag{6}$$

Note that in these expressions, losses in the inductors have been taken into account and modeled by pure resistances (r_1 and r_2, respectively, for inductors L_1 and L_2).

As the current through L_1 experiences a decreasing rate, it eventually equals those of L_2. In that case, the absolute voltage across L_2 becomes less than $V_{\text{DC}}/2$ and the rectifier bridge is blocked. This corresponds to states ⓒ and ⓗ, where the same current flows through L_1 and L_2. The corresponding states matrices are then given by

$$\mathbf{A_c} = \mathbf{A_h} = \begin{bmatrix} 0 & -\frac{1}{C_0} & 0 \\ \frac{1}{L_1+L_2} & -\frac{r_1+r_2}{L_1+L_2} & 0 \\ \frac{1}{L_1+L_2} & -\frac{r_1+r_2}{L_1+L_2} & 0 \end{bmatrix}$$
$$\mathbf{B_c} = \mathbf{B_h} = \begin{bmatrix} \frac{\alpha}{C_0} & 0 \\ 0 & 0 \\ 0 & 0 \end{bmatrix}. \tag{7}$$

It can be noted that in that case, the instantaneous natural inversion frequency changes from $1/(2\pi\sqrt{L_1 C_0})$ to $1/(2\pi\sqrt{(L_1+L_2)C_0})$ (not taking into account the effect of losses), as the voltage across L_2 is no longer clipped by the rectifier voltage.

As the current decreases, however, its absolute rate reaches once again the maximum rate allowed through L_2 (voltage clipping to $\mp V_{\text{DC}}$ - states ⓓ and ⓘ). In that case, the state matrices yield

$$\mathbf{A_d} = \mathbf{A_i} = \begin{bmatrix} 0 & -\frac{1}{C_0} & 0 \\ \frac{1}{L_1} & -\frac{r_1}{L_1} & 0 \\ 0 & 0 & -\frac{r_2}{L_2} \end{bmatrix}$$
$$\mathbf{B_d} = \begin{bmatrix} \frac{\alpha}{C_0} & 0 \\ 0 & \frac{1}{2L_1} \\ 0 & -\frac{1}{2L_2} \end{bmatrix}, \mathbf{B_i} = \begin{bmatrix} \frac{\alpha}{C_0} & 0 \\ 0 & -\frac{1}{2L_1} \\ 0 & \frac{1}{2L_2} \end{bmatrix}. \tag{8}$$

Finally, as the piezovoltage inversion stops (cancellation of the current through L_1), residual current may still flow through L_2 and the rectification stage (states ⓔ and ⓙ). The associated state matrices are given by

$$\mathbf{A_e} = \mathbf{A_j} = \begin{bmatrix} 0 & 0 & 0 \\ 0 & 0 & 0 \\ 0 & 0 & -\frac{r_2}{L_2} \end{bmatrix}$$
$$\mathbf{B_e} = \begin{bmatrix} \frac{\alpha}{C_0} & 0 \\ 0 & 0 \\ 0 & -\frac{1}{2L_2} \end{bmatrix}, \quad \mathbf{B_j} = \begin{bmatrix} \frac{\alpha}{C_0} & 0 \\ 0 & 0 \\ 0 & \frac{1}{2L_2} \end{bmatrix}. \tag{9}$$

B. State Switching Conditions and Derivation of Other Quantities

While the previous analysis allowed to derive the governing equation for each state, this section discusses the conditions for changing from one state to another one. To this end, the voltage V_{L2} across inductor L_2 is also considered

$$V_{L2} = L_2 \dot{I}_{L2} + r_2 I_{L2}. \tag{10}$$

Additionally, the previously exposed model being intended to be solved through numerical iterations, the variables are here considered as discrete. However, for the sake of clarity, the discrete step index is omitted.

From the open circuit stage ⓐ (*resp.* ⓕ), the condition to enter the switching state ⓑ (*resp.* ⓖ) is either based on the velocity or the voltage. The SSHI is indeed based on connecting the switching circuit on velocity cancellation ($\dot{u} = 0$), but practically, its implementation relies, in a equivalent way, on the detection of extremal voltage.

Once in state ⓑ (*resp.* ⓖ), where the voltage across L_2 is clipped by $+V_{\text{DC}}/2$ (*resp.* $-V_{\text{DC}}/2$) and with current from the PZT flowing through L_1, the absolute current increase rate through L_2 is, thus, limited and is less than the absolute current through L_1 (see Fig. 2). The end of this state is not only determined by V_{L2} but also considering the current flowing through the diodes D_1 and D_2, which should be direct. Hence,

the following conditions should be satisfied to stay in state ⓑ (*resp.* ⓖ):

$$\begin{cases} |V_{L2}| \geq \frac{V_{\rm DC}}{2} \\ \operatorname{sgn}(V_{L2}) \times (I_{L1} - I_{L2}) \geq 0 \end{cases} \tag{11}$$

with $\operatorname{sgn}(x)$ the signum function of the variable x. In (11), the second condition relates the current direction in the diodes (the signum of V_{L2} allowing determining which diode conducts, while the current differentiation gives the current direction). When one of these conditions is no longer met, the circuit enters in state ⓒ(*resp.* ⓗ).

When operating in state ⓒ(*resp.* ⓗ), the rectification stage is blocked, and the inversion is solely done through L_1 and L_2 (the inversion frequency is, thus, reduced compared to states ⓑ, ⓓ, ⓘ and ⓖ). The condition to stay in this state ⓒ(*resp.* ⓗ) is to have a voltage across L_2, V_{L2}, higher than $-V_{\rm DC}/2$ (*resp.* lower than $+V_{\rm DC}/2$)

$$|V_{L2}| \leq \frac{V_{\rm DC}}{2}. \tag{12}$$

As soon as this condition is no longer satisfied, the circuit enters in state ⓓ (*resp.* ⓘ), where the inversion is performed with one of the rectifier branch conducting. Such a configuration keeps valid as long as the current through the switch (or equivalently current flowing out of the piezoelectric element or current flowing through inductance L_1) does not cancel.

As the current through L_1 cancels the piezovoltage inversion process is terminated but residual current in L_2 yields a continuation of the diode bridge conduction (state ⓔ - *resp.* ⓙ). This conduction lasts until the absolute voltage across L_2, namely $|V_{L2}|$, is greater than $V_{\rm DC}/2$ and as a direct current flows through D_2 (*resp.* D_1), yielding same conditions as in (11). Once terminated, the circuit goes back to original configuration (state ⓕ- *resp.* ⓐ).

IV. Numerical Discussion

This section proposes to discuss the performance of the sp-SSHI architecture under various parameter configurations. Assuming the PZT driven by a monochromatic signal of frequency f, harvested energy for one switching cycle $W_{\rm harv}$ can be obtained through one of the following relationships (respectively, referring to the positive and negative piezovoltage switching):

$$\begin{cases} W_{\rm harv} = \frac{V_{DC}}{2} \int_{t_b|_{\rm beg}}^{t_e|_{\rm end}} |I_h(t)|\, dt \\ W_{\rm harv} = \frac{V_{DC}}{2} \int_{t_g|_{\rm beg}}^{t_j|_{\rm end}} |I_h(t)|\, dt \end{cases} \tag{13}$$

where $t_x|_{\rm beg}$ refers to the time instant when state x begins and $t_y|_{\rm end}$ the time instant when the state y consecutive to x finishes. $I_h(t)$ is besides defined as the current flowing through the harvesting stage

$$I_h(t) = I_{L1}(t) - I_{L2}(t). \tag{14}$$

As two harvesting processes occur per period (respectively, on positive and negative voltage values), the total harvested power $P_{\rm harv}$ turns to

$$P_{\rm harv} = 2 f W_{\rm harv}. \tag{15}$$

For comparison purposes, other typical circuits consisting of standard interface (sole rectifier bridge with smoothing capacitor [31]), parallel SSHI (rectifier with smoothing capacitor and switching unit in parallel to it [6], [7]) and series SSHI (rectifier with smoothing capacitor and switching unit in series between the PZT and rectifier [6], [8]) may be considered. The associated power expressions, in the case of full-wave voltage doublers, are given by

$$\begin{aligned} P_{\rm stand} &= f V_{\rm DC} \left(2\alpha u_M - C_0 V_{\rm DC}\right) \\ P_{p-\rm SSHI} &= f V_{\rm DC} \left(2\alpha u_M - \tfrac{1-\gamma}{2} C_0 V_{\rm DC}\right) \\ P_{s-\rm SSHI} &= \tfrac{1+\gamma}{1-\gamma} f V_{\rm DC} \left(2\alpha u_M - C_0 V_{\rm DC}\right) \end{aligned} \tag{16}$$

where γ denotes the voltage inversion factor

$$\gamma = e^{-\frac{\pi}{2Q_i}} \quad , \quad Q_i = \frac{1}{r}\sqrt{\frac{L}{C_0}} \tag{17}$$

with L and r are the respective inductor value and equivalent loss resistor in the switching unit (including inductor losses), respectively. Obtained results in terms of output voltages and powers are depicted in Fig. 4 for several cases of adimensional inductance values defined as

$$\tilde{L}_x = L_x C_0 \left(2\pi f\right)^2 \tag{18}$$

with $\tilde{\chi}$ is the adimensional counterpart of the parameter χ, and x is the subscript associated to the parameter.[1] Also, constant electrical quality factor Q_i has been considered for the inductors, which can be potentially varied from one simulation to another. In practical application, however, and because some parts of the switching event would experience larger inversion frequency as L_1 decreases (keeping $L_1 + L_2$ constant), the electrical quality factor may slightly increase and so would be the power. Hence, presented results may be slightly underestimated. Load values have been obtained by dividing the squared rectified voltage by the calculated associated power output. Finally, for an easier and general comparison, the powers, voltages, and loads have been normalized to the respective maximal power, optimal voltage, and optimal load in the standard case.

These results demonstrates that, for relatively high L_2/L_1 inductance ratio and moderate to high electrical quality factor, a significant harvested power can be achieved over a wide voltage/load range, combining the advantage of SSHI in terms of power gains and SECE in terms of power robustness facing load variations. However, the maximal voltage that can be achieved in quasi open-circuit condition keeps lower than the parallel SSHI. Under the considered conditions (constant electrical quality factor for each plot), it can be noticed that the total inductance value has almost no impact on the power curves, while the inductance ratio plays a great role. While all the curves starts following the response of series SSHI, increasing the load (or rectified voltage) may induce a second peak in terms of power. Especially, for relatively high value of inductance L_2 (hence with significant energy stored in this inductance), the second peak is getting closer to the parallel SSHI optimal point as

[1]Note that thanks to the switching principles, the normalized inductance value is much less than the unit (the latter corresponding to passive impedance matching), denoting a more realistic implementation.

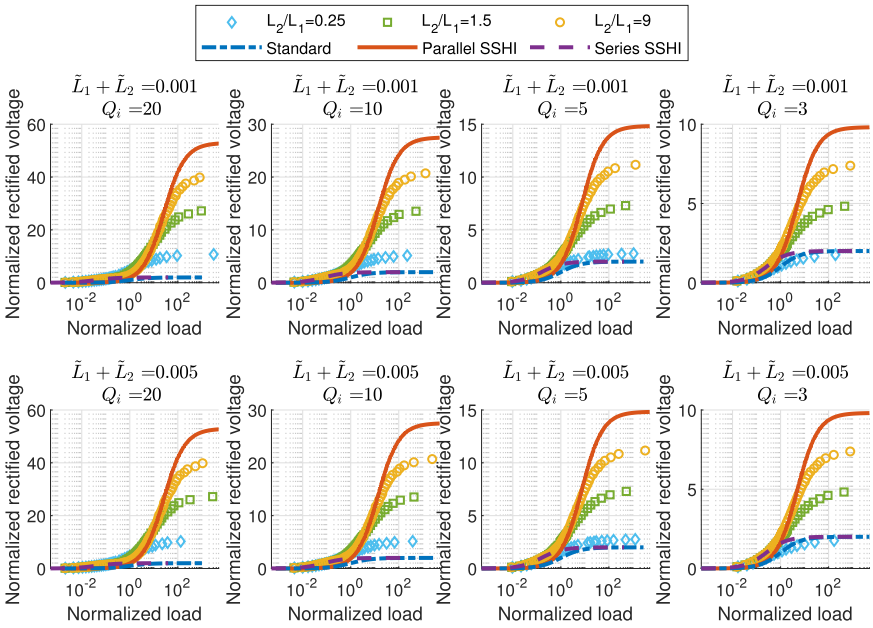

(a)

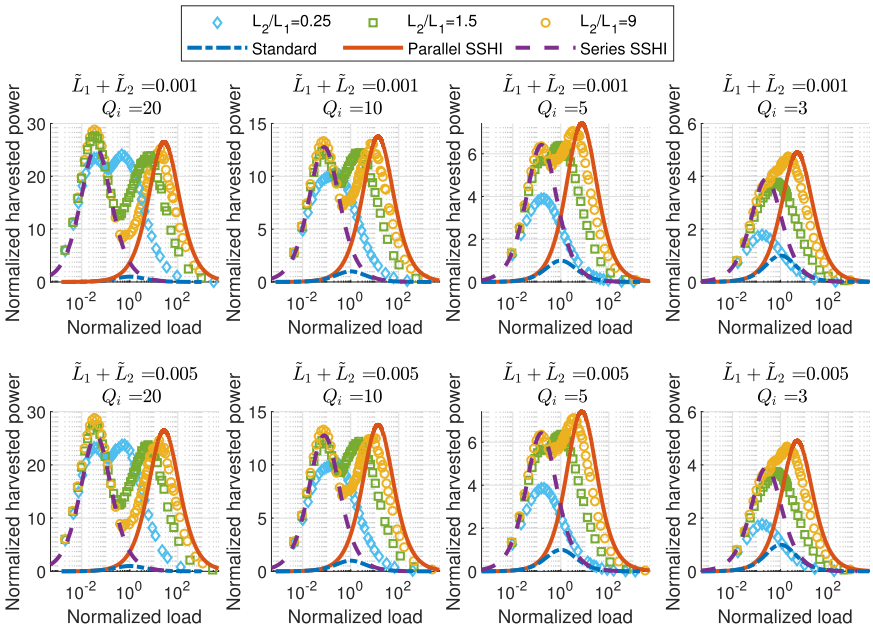

(b)

Fig. 4. Obtained voltages and powers from numerical resolution. (a) Voltage as a function of load. (b) Power as a function of load.

L_2 value increases. This, therefore, permits a wide load range with a significant output power, although a relatively limited well appears as the electrical quality factor (or equivalently the inversion factor) increases.

In order to evaluate the electrostatic energy available on the piezoelectric energy as well as the conversion enhancement enabled by the switching process, Fig. 5 depicts the voltage just before the energy extraction. Hence, it can be noticed that the latter is particularly high for low load values in the case of series SSHI, and for high load values for parallel SSHI. This is explained by the fact that the voltage inversion is done with respect to half the rectified voltage in the former case, and by the voltage clipping to half the rectified voltage in the latter approach. Hence, this may yield significant losses, especially related to diode threshold voltage, when the load is high for the series SSHI (as almost no inversion event occurs) and for low load values in the case of parallel SSHI (the voltage clipping being mostly induced by the diodes). In the case of sp-SSHI, however, thanks to the hybrid approach enabled by the two inductors, it can be noticed that the piezovoltage remains at a rather high value over the full load range. Hence, this not only denotes the better ability for enhancing the energy conversion

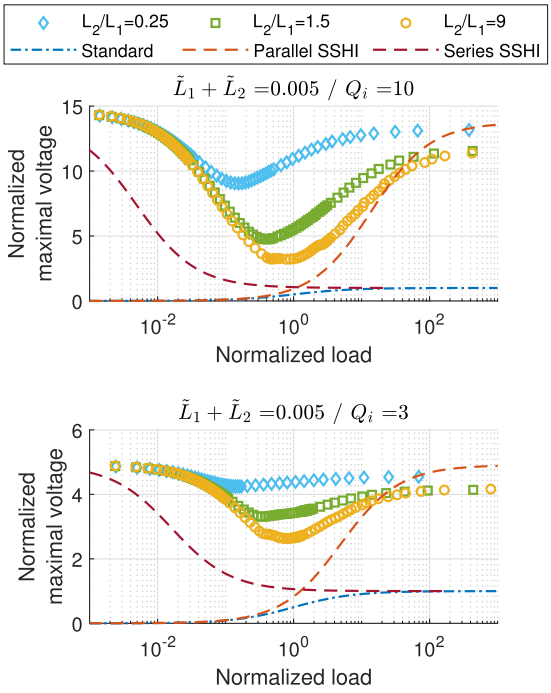

Fig. 5. PZT voltage just before switching.

but also permits to mitigate the conduction losses during charge transfer to the storage stage. Also, thanks to the supplementary energy stored in L_2 that is then released as the inversion event is terminated, natural discharge to the storage stage happens, with an overvoltage peak that allows bypassing the diode thresholds.

The inductance values also impact the inversion time and thus required timing and associated power consumption. Additionally, contrary to previous SSHI and SECE approaches, changing the rectified voltage, or equivalently the load, yields a modification of the inversion time (steps ⓑ to ⓓ and ⓖ to ⓘ in Fig. 2). More precisely, the voltage being clipped in steps ⓑ, ⓓ, ⓖ, and ⓘ, only inductor L_1 contributes to the inversion time, while both inductors intervene in steps ⓒ and ⓗ. Hence, the total inversion time t_i is comprised between the two boundaries defined by the total effective inductor as

$$\pi\sqrt{L_1 C_0} \leq t_i \leq \pi\sqrt{(L_1 + L_2)\, C_0} \tag{19}$$

where the lower boundary corresponds to low voltages/loads (piezovoltage almost always clipped) and the upper one to large values of voltage or load (almost no clipping). Hence, reducing the inductance values may allow reduced inversion time, which however can significantly increase the losses, especially due to the higher current peak caused by faster switching process (notably due to nonlinear effects, such as iron losses). These losses besides vary with the load or voltage, which change the inversion time and peak current. Nonetheless, typical implementations of self-powered switches [11]–[13] rely on a diode for stopping the inversion (which occurs when the current flowing out the piezoelement cancels). Therefore, even if the inversion time may vary, this allows an automatic adjustment of the switching time.

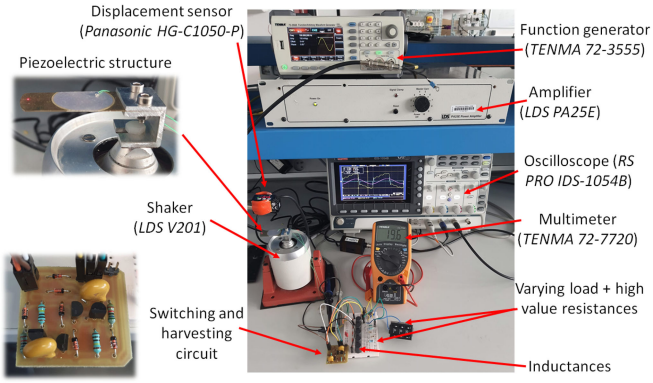

Fig. 6. Schematic diagram of the experimental setup.

Another very interesting feature of the sp-SSHI is its ability to provide an outstanding power boost at low voltage/load values, even higher than the conventional parallel or series SSHI for a significant value of the electrical quality factor. Such a unique feature is explained by the additional energy stored in inductance L_2, especially at low rectified voltage/load. Indeed, while the voltage clipping yields charges flowing to the storage stage (as in the series SSHI case), some extra energy is also accumulated by L_2, and then released to the storage in the next steps (*e.g.*, states ⓔ and ⓙ). This energy therefore adds up to the former one, thus leading to a substantial gain compared to the traditional SSHI approaches. As the rectified voltage/load are increasing, the structure gets closer to the parallel SSHI still through L_2, and most of the current flowing through this inductance is used for voltage flipping (reduced voltage clipping).

V. Experimental Validation

Based on the previous concept and analysis, this section aims at experimentally assessing the real performance of the proposed circuit. In order to reflect as much as possible realistic implementation, the device will be made totally autonomous through the use of a self-powered switching unit.

A. Experimental Setup

The experimental device (see Fig. 6) is made of a piezoelectric cantilever beam obtained by cutting two commercial buzzers (RS PRO 837-7844). The two buzzer pieces were then bonded onto each other through their substrate. The output terminal of each beam has been connected in serial configuration. This electromechanical structure is mounted on an electrodynamic shaker fed by a function generator through a power amplifier that applies a base acceleration on the piezoelectric system. The excitation frequency is set to 100 Hz, which is slightly off resonance, and the tip displacement magnitude is kept constant to 120 μm peak and monitored using a laser optical sensor. Electrical signals (piezovoltage, function generator output voltage and displacement sensor output) are observed through an oscilloscope, while dc output voltage is monitored using a multimeter.

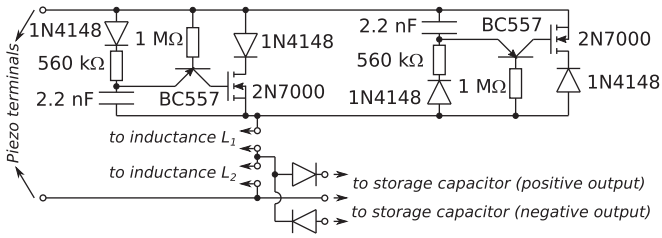

Fig. 7. Implementation of the self-powered switch.

TABLE I
MODEL PARAMETERS

Parameter	Value
Clamped capacitance C_0	44.4 nF
Force factor α	1.9 mN.V^{-1}
Electrical quality factor Q_i	3.52

The self-powered switch is implemented following the initial proposal made by Richard *et al.* [11], [12], as depicted in Fig. 7. While it is less compact than the configuration proposed by Eltamaly and Addoweesh in [13], which advantageously uses some transistors for two functions (diode for filtering during one half period, comparator for the other half), it allows better handling of high voltages. Five inductors (RL181S-104J-RC, manufactured by Bourns), each with a value of 100 mH, have been connected serially, with access to each intermediate node to connect the harvesting stage in the sp-SSHI configuration. For series and parallel SSHI, all of the five inductors were kept in the inversion circuit for fair comparison. Two 47 μF/25 V capacitors, picked from CCC-14 kit from Nova, were selected as smoothing capacitors. The output of the harvesting stage was then connected to a varying resistive load. In the case of loads greater than 1 MΩ, the voltage was monitored on a series 1 MΩ resistor (that was taken into account in the total load value) in order to ensure a negligible effect of the voltmeter input impedance (typically 10 MΩ), and the total rectifier voltage was derived using standard resistive divider formula.

Prior to power measurements, model identification has been performed. Obtained parameters are listed in Table I. The inversion factor γ was obtained with the harvesting stage disconnected, allowing the derivation of the electrical quality factor according to (17).

B. Result and Discussions

Based on the previously exposed experimental device and set-up, energy harvesting capabilities were assessed. The influence of the parallel to series inductance ratio was considered, while keeping the total inductance constant (including in the SSHI cases). Results are exposed in Fig. 8.

These results, therefore, confirm the capabilities of the sp-SSHI for providing similar performance than the series and parallel SSHI in terms of maximal output power, while allowing a wide range of operating loads (or equivalently, of states of the connected electronic device). While the series and parallel SSHI half-power load range are roughly [10 kΩ, 300 kΩ] and

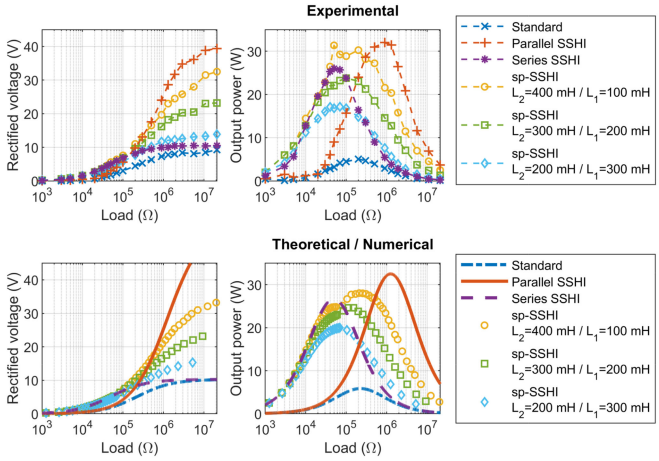

Fig. 8. Experimental voltages and harvested powers and comparison with numerical and theoretical resolutions.

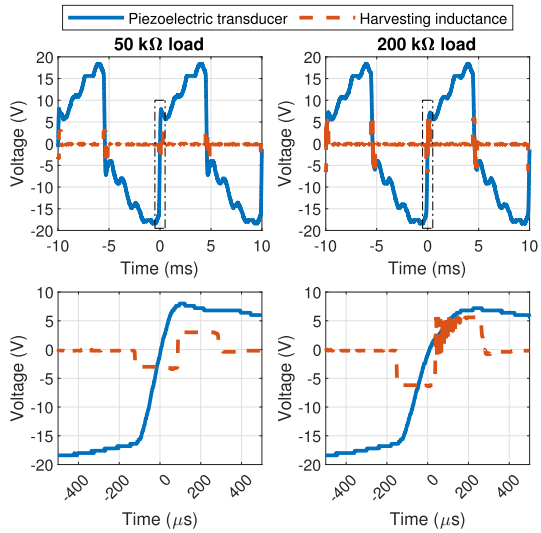

Fig. 9. Waveforms for $L_1 = 100$ mH and $L_2 = 400$ mH with 50 kΩ and 200 kΩ loads.

[100 kΩ, 4 MΩ], respectively, it is gaining a factor of 5 when using the sp-SSHI [10 kΩ, 2 MΩ], hence covering more than two decades. It is also noteworthy that experimentally obtained results in terms of power for the sp-SSHI are better than in the theoretical case, which may be explained by higher electrical quality factor as the switching frequency increases when the voltage across L_2 is clipped.

Such an effect actually leads to two voltage peaks that appear even for relatively low values of the electrical quality factor. Fig. 9 shows the voltage waveforms obtained in the case of $L_2 = 400$ mH and $L_1 = 100$ mH for the two power peaks. Hence, it can be noticed that for the lowest optimal load (50 kΩ), three harvesting events occur (voltage clipping for each polarity, with the second one continuing after the switching event) with an almost instantaneous change from one harvesting event to the other one, while for the highest optimal load (200 kΩ), almost only one harvesting event arises.

TABLE II
COMPARISON OF ENERGY HARVESTING TECHNIQUES

	Power (w.r.t. standard case)	Load bandwidth (w.r.t. optimal load in standard case)	Self-powering capabilities
Standard ([6])	1	[0.2; 5]	Straightforward
Parallel SSHI ([6, 7])	7-10	[0.5; 20]	Easy
Series SSHI ([6])	6-9	[0.05; 1.5]	Easy
SECE ([20])	3-4	$[-\infty, \infty]$ theoretically 3 decades practically[2]	Complex
Hybrid SSHI ([25])	7-10	[0.5; 500][3]	Easy[4]
DSSH ([23]) / ESSH ([24])	5-7	Similar to SECE	Very complex
SICE ([27])	6-8	Similar to SECE	Very complex
sp-SSHI	8-10	[0.05; 10]	Easy

[1]Exact normalized range varies according to voltage value.
[2]With significant power well within range.
[3]However, the need of a transformer yields a bulky implementation.

VI. CONCLUSION

This article introduced an architecture aiming at improving the energy harvesting performance of piezoelectric microgenerator. By splitting the inductance used in the SSHI approach and connecting the harvesting stage (rectifier) at the middle point, a hybrid interface between series and parallel configuration is achieved. One particular aspect of such an approach is that the inductance in parallel with the rectification stage permits a supplementary energy release step after the switching event. The performance analysis of the circuit, based on state-space simulations and experimental investigations, demonstrated that a wider range of operating voltage or resistive load is achieved. Additionally, under particular conditions (limited losses and high ratio of the parallel inductance over the series one), the proposed techniques permits and outstanding gain, even bypassing the case of parallel SSHI. Further works may consider the investigation of the damping induced by such a technique, as well as integrated solutions limiting the losses in the energy transfer steps and inversion events.

Table II proposes as a general synthesis a comparison between the sp-SSHI technique and other typical approaches. Hence, it can be observed that the proposed method permits a high relative power while ensuring a relatively important load bandwidth and simple and rather compact self-powered implementation. This, therefore, provides a very attractive means of harvesting energy.

CONFLICT OF INTEREST

The present manuscript has neither been presented at a conference nor submitted elsewhere previously.

REFERENCES

[1] J. VanZwol, "Designing battery packs for thermal extremes," *Power Electron. Technol.*, vol. 32, pp. 40–45, Jul. 2006.

[2] V. Knap, D.-I. Stroe, M. Swierczynski, R. Teodorescu, and E. Schaltz, "Investigation of the self-discharge behavior of Lithium-Sulfur batteries," *J. Electrochem. Soc.*, vol. 163, no. 6, pp. A911–A916, 2016.

[3] F. K. Shaikh and S. Zeadally, "Energy harvesting in wireless sensor networks: A comprehensive review," *Renewable Sustain. Energy Rev.*, vol. 55, pp. 1041–1054, 2016.

[4] D. Newell and M. Duffy, "Review of power conversion and energy management for low-power, low-voltage energy harvesting powered wireless sensors," *IEEE Trans. Power Electron.*, vol. 34, no. 10, pp. 9794–9805, Oct. 2019.

[5] C. Wei and X. Jing, "A comprehensive review on vibration energy harvesting: Modelling and realization," *Renewable Sustain. Energy Rev.*, vol. 74, pp. 1–18, 2017.

[6] E. Lefeuvre, A. Badel, C. Richard, L. Petit, and D. Guyomar, "A comparison between several vibration-powered piezoelectric generators for standalone systems," *Sensors Actuators A, Phys.*, vol. 126, pp. 405–416, 2006.

[7] D. Guyomar, A. Badel, E. Lefeuvre, and C. Richard, "Toward energy harvesting using active materials and conversion improvement by nonlinear processing," *IEEE Trans. Ultrason. Ferroelectr. Freq. Control.*, vol. 52, no. 4, pp. 584–595, Apr. 2005.

[8] G. W. Taylor, J. R. Burns, S. M. Kammann, W. B. Powers, and T. R. Welsh, "The energy harvesting eel: A small subsurface Ocean/River power generator," *IEEE J. Ocean. Eng.*, vol. 26, no. 4, pp. 539–547, Oct. 2001.

[9] B. Zhao, K. Zhao, X. Wang, J. Liang, and Z. Chen, "Series synchronized triple bias-flip circuit: Maximizing the usage of single storage capacitor for piezoelectric energy harvesting enhancement," *IEEE Trans. Power Electron.*, vol. 36, no. 6, pp. 6787–6796, Jun. 2021.

[10] M. Lallart, W.-J. Wu, L. Yan, and S.-W. Hung, "Inductorless synchronized switch harvesting using a piezoelectric oscillator," *IEEE Trans. Power Electron.*, vol. 35, no. 3, pp. 2585–2594, Mar. 2020.

[11] C. Richard, D. Guyomar, and E. Lefeuvre, "Self-powered electronic breaker with automatic switching by detecting maxima or minima of potential difference between its power electrodes," Patent #PCT/FR2005/003000, 2007.

[12] M. Lallart and D. Guyomar, "Optimized self-powered switching circuit for non-linear energy harvesting with low voltage output," *Smart Mater. Struct.*, vol. 17, 2008, Art. no. 035030.

[13] A. M. Eltamaly and K. E. Addoweesh, "A novel self-power SSHI circuit for piezoelectric energy harvester," *IEEE Trans. Power Electron.*, vol. 35, no. 3, pp. 2585–2594, Mar. 2020.

[14] Z. Chen, Y. Xia, G. Shi, X. Wang, H. Xia, and Y. Ye, "Self-powered multi-input serial SSHI interface circuit with arbitrary phase difference for piezoelectric energy harvesting," *IEEE Trans. Power Electron.*, vol. 36, no. 8, pp. 9183–9192, Aug. 2021.

[15] X. Wang *et al.*, "A self-powered rectifier-less synchronized switch harvesting on inductor interface circuit for piezoelectric energy harvesting," *IEEE Trans. Power Electron.*, vol. 36, no. 8, pp. 9149–9159, Aug. 2021.

[16] H. Xia *et al.*, "Self-powered dual-inductor MI-PSSHI-VDR interface circuit for Multi-PZTs energy harvesting," *IEEE Trans. Power Electron.*, vol. 37, no. 4, pp. 3753–3762, Apr. 2022.

[17] G. K. Ottman, H. F. Hofmann, and G. A. Lesieutre, "Optimized piezoelectric energy harvesting circuit using step-down converter in discontinuous conduction mode," *IEEE Trans. Power Electron.*, vol. 18, no. 2, pp. 696–703, Mar. 2003.

[18] E. Lefeuvre, D. Audigier, C. Richard, and D. Guyomar, "Buck-boost converter for sensorless power optimization of piezoelectric energy harvester," *IEEE Trans. Power Electron.*, vol. 22, no. 5, pp. 2018–2025, Sep. 2007.

[19] M. Lallart and D. J. Inman, "Low-cost integrable tuning-free converter for piezoelectric energy harvesting optimization," *IEEE Trans. Power Electron.*, vol. 25, no. 7, pp. 1811–1819, Jul. 2010.

[20] E. Lefeuvre, A. Badel, C. Richard, and D. Guyomar, "Piezoelectric energy harvesting device optimization by synchronous electric charge extraction," *J. Intell. Mater. Syst. Struct.*, vol. 16, pp. 865–876, 2005.

[21] X. Wang *et al.*, "Multi-input SECE based on buck structure for piezoelectric energy harvesting," *IEEE Trans. Power Electron.*, vol. 36, no. 4, pp. 3638–3642, Apr. 2021.

[22] A. Romani, M. Filippi, and M. Tartagni, "Micropower design of a fully autonomous energy harvesting circuit for arrays of piezoelectric transducers," *IEEE Trans. Power Electron.*, vol. 29, no. 2, pp. 729–739, Feb. 2014.

[23] M. Lallart, L. Garbuio, L. Petit, C. Richard, and D. Guyomar, "Double synchronized switch harvesting (DSSH): A. new energy harvesting scheme for efficient energy extraction," *IEEE Trans. Ultrason., Ferroelectr. Freq. Control*, vol. 55, no. 10, pp. 2119–2130, Oct. 2008.

[24] H. Shen, J. Qiu, H. Ji, K. Zhu, and M. Balsi, "Enhanced synchronized switch harvesting: A new energy harvesting scheme for efficient energy extraction," *Smart Mater. Struct.*, vol. 19, no. 11, 2010, Art. no. 115017.

[25] M. Lallart, C. Richard, L. Garbuio, L. Petit, and D. Guyomar, "High efficiency, wide load bandwidth piezoelectric energy scavenging by a hybrid nonlinear approach," *Sensors Actuators A, Phys.*, vol. 165, no. 2, pp. 294–302, 2011.
[26] Y. Wu, A. Badel, F. Formosa, W. Liu, and A. Agbossou, "Piezoelectric vibration energy harvesting by optimized synchronous electric charge extraction," *J. Intell. Mater. Syst. Struct.*, vol. 24, no. 12, pp. 1445–1458, 2012.
[27] M. Lallart, W.-J. Wu, Y. Hsieh, and L. Yan, "Synchronous inversion and charge extraction (SICE): A hybrid switching interface for efficient vibrational energy harvesting," *Smart Mater. Struct.*, vol. 26, no. 11, 2017, Art. no. 115012.
[28] H. Xia, Y. Xia, G. Shi, Y. Ye, Z. Chen, and Q. Jiang, "A self-powered S-SSHI and SECE hybrid rectifier for PE energy harvesters: Analysis and experiment," *IEEE Trans. Power Electron.*, vol. 36, no. 2, pp. 1680–1692, Feb. 2021.
[29] W. P. Mason, *Electromechanical Transducers and Wave Filters*. Princeton NJ, USA: Van Nostrand, 1948.
[30] A. Badel, M. Lagache, D. Guyomar, E. Lefeuvre, and C. Richard, "Finite element and simple lumped modeling for flexural nonlinear semi-passive damping," *J. Intell. Mater. Syst. Struct.*, vol. 18, pp. 727–742, 2007.
[31] G. K. Ottman, H. F. Hofmann, A. C. Bhatt, and G. A. Lesieutre, "Adaptive piezoelectric energy harvesting circuit for wireless remote power supply," *IEEE Trans. Power Electron.*, vol. 17, no. 5, pp. 669–676, Sep. 2002.

Mickaël Lallart was born in 1983. He received the Graduate degree in electrical engineering and the Ph.D. degree in electronics, electrotechnics, and automatics from the Institut National des Sciences Appliquées de Lyon (INSA-Lyon), Lyon, France, in 2006 and 2008, respectively.

He worked with the Laboratoire de Génie Electrique et Ferroélectricité (LGEF). After completing, a postdoctoral fellowship with the Center for Intelligent Material Systems and Structures (CIMSS) in Virginia Tech, Blacksburg, VA, USA, in 2009, he has been hired as an Associate Professor with the Laboratoire de Génie Electrique et Ferroélectricité, and has been appointed as a Full-Time Professor in 2019. Since 2006, he authored or coauthored more than 100 papers in international peer-reviewed journals and authored more than 90 conference papers including 11 personally invited talks and 3 plenary talks. He edited 6 books and participated to 9 book chapters and reviewed more than 250 manuscripts for various journals.

Dr. Lallart was the recipient of an invited JSPS research fellowship in Tohoku University, Sendai, Japan, in 2019–2020, and held an invited Adjunct Researcher position in NorthWestern Polytechnical University (NPU), Xi'an, China, in 2018–2020. He was a PI or key partner of National and International Academic Projects funded by French National Research Agency or European Union for instance, and participated to several industrial collaborations as well.